Published in final edited form as:
Cell. 2010 September 17; 142(6): 857–867. doi:10.1016/j.cell.2010.08.014.

An iron-export ferroxidase activity of β-amyloid protein precursor is inhibited by zinc in Alzheimer's Disease

James A. Duce[1], **Andrew Tsatsanis**[1], **Michael A. Cater**[1,^], **Simon A. James**[1], **Elysia Robb**[1], **Krutika Wikhe**[1], **Su Ling Leong**[3,4], **Keyla Perez**[1,3,4], **Timothy Johanssen**[4], **Mark A. Greenough**[1,2], **Hyun-Hee Cho**[5], **Denise Galatis**[3], **Robert D. Moir**[6], **Colin L. Masters**[1], **Catriona McLean**[7], **Rudolph E. Tanzi**[6], **Roberto Cappai**[3,4], **Kevin J. Barnham**[1,3,4], **Giuseppe D. Ciccotosto**[1,3,4], **Jack T. Rogers**[4,5,*], and **Ashley I. Bush**[1,3,*]

[1] Mental Health Research Institute, The University of Melbourne, Parkville, Victoria 3052, Australia

[2] Department of Genetics, The University of Melbourne, Victoria 3010, Australia

[3] Department of Pathology, The University of Melbourne, Victoria 3010, Australia

[4] Bio21 Molecular Science and Biotechnology Institute, The University of Melbourne, Victoria 3010, Australia

[5] Neurochemistry Laboratory, Department of Psychiatry, Harvard Medical School, Massachusetts General Hospital, Charlestown, MA, 02129, USA

[6] Genetics and Aging Research Unit, Massachusetts General Hospital, Charlestown, MA, 02129, USA

[7] Department of Anatomical Pathology, Alfred Hospital, Melbourne, Victoria 3004 Australia

Summary

Alzheimer's Disease (AD) is complicated by pro-oxidant intraneuronal Fe^{2+} elevation as well as extracellular Zn^{2+} accumulation within amyloid plaque. We found that the AD β-amyloid protein precursor (APP) possesses ferroxidase activity mediated by a conserved H-ferritin-like active site, which is inhibited specifically by Zn^{2+}. Like ceruloplasmin, APP catalytically oxidizes Fe^{2+}, loads Fe^{3+} into transferrin, and has a major interaction with ferroportin in HEK293T cells (that lack ceruloplasmin) and in human cortical tissue. Ablation of APP in HEK293T cells and primary neurons induces marked iron retention, whereas increasing APP695 promotes iron export. Unlike normal mice, APP−/− mice are vulnerable to dietary iron exposure, which causes Fe^{2+} accumulation and oxidative stress in cortical neurons. Paralleling iron accumulation, APP ferroxidase activity in AD post-mortem neocortex is inhibited by endogenous Zn^{2+}, which we demonstrate can originate from Zn^{2+}-laden amyloid aggregates and correlates with Aβ burden. Abnormal exchange of cortical zinc may link amyloid pathology with neuronal iron accumulation in AD.

Correspondence to abush@mhri.edu.au or jtrogers@rics.bwh.harvard.edu.
*These authors shared senior authorship duties.
^ Current address: Research Division, The Peter MacCallum Cancer Centre, St. Andrew's Place, East Melbourne, Victoria 3002, Australia

Supplemental experimental procedures can be found online.

Introduction

In Alzheimer's disease (AD), Zn^{2+} collects with β-amyloid (Aβ) in hallmark extracellular plaques (Adlard et al., 2008; Cherny et al., 1999; Lee et al., 2002; Lovell et al., 1998; Miller et al., 2006; Suh et al., 2000), adjacent to neocortical neurons filled with pro-oxidant Fe^{2+} (Bartzokis et al., 1994a; Bartzokis et al., 1994b; Bartzokis and Tishler, 2000; Honda et al., 2005). The elevated neuronal iron exacerbates the pervasive oxidative damage that characterizes AD, and may foster multiple pathologies including tau-hyperphosphorylation and neurofibrillary tangle formation (Honda et al., 2005; Smith et al., 1997; Yamamoto et al., 2002), but the cause of this neuronal iron elevation is unknown.

Aβ is derived from a broadly-expressed type I transmembrane protein precursor (APP) of uncertain function, and constitutively cleaved into various fragments. The 5′UTR of APP mRNA possesses a functional Iron-Responsive Element (IRE) stemloop with sequence homology to the IREs for ferritin and transferrin receptor (TfR) mRNA (Rogers et al., 2002). APP translation is thus responsive to cytoplasmic free iron levels (the Labile Iron Pool, LIP), which also govern the binding of Iron Regulatory Proteins (IRPs) to ferritin and TfR mRNA in a canonical cis-trans iron regulatory system (Klausner et al., 1993). When cellular iron levels are high, translation of APP and the iron-storage protein ferritin is increased (Rogers et al., 2002), while RNA for the iron importer TfR is degraded.

Ferroxidases prevent oxidative stress caused by Fenton and Haber-Weiss chemistry by oxidizing Fe^{2+} to Fe^{3+}. Losses of ferroxidase activities cause pathological Fe^{2+} accumulation and neurodegenerative diseases, such as aceruloplasminemia where mutation of the multi-copper ferroxidase ceruloplasmin (Cp) leads to glial iron accumulation and dementia (Chinnery et al., 2007; Harris et al., 1995; Mantovan et al., 2006; Patel et al., 2002). Iron-export ferroxidases Cp and hephaestin interact with ferroportin and facilitate the removal (e.g. by transferrin) of cytoplasmic iron translocated to the surface by ferroportin (De Domenico et al., 2007). Their expression is cell-specific (e.g. Cp in glia, hephaestin in gut epithelia), but an iron-export ferroxidase for neocortical neurons is unknown (Klomp et al., 1996). Cp is expressed in GPI-anchored and soluble forms (De Domenico et al., 2007; Jeong and David, 2003; Patel et al., 2002). APP similarly is expressed in transmembrane and secreted forms. We explored whether APP is a ferroxidase, and in turn has a role in neuronal iron export – an activity consistent with APP translation being responsive to iron levels. We also tested whether, in AD, APP ferroxidase activity is altered in a manner linked to the accumulation of its Aβ derivative in plaque pathology.

RESULTS

APP695 possesses ferroxidase activity similar to ceruloplasmin

We noted that APP possesses a REXXE ferroxidase consensus motif (Gutierrez et al., 1997) as found in the ferroxidase active site of H-ferritin (Figure 1A, B). This evolutionarily conserved motif is not present in paralogs APLP1 or 2 (Figure1B). There is good structural homology between the known 3D structures of H-ferritin (Lawson et al., 1991) and the REXXE-region of the E2 domain of APP (Wang and Ha, 2004), with low root mean square deviation (0.4 A) when overlaying backbone atoms of the α-helical H-ferritin catalytic site (residues 52–67) with the corresponding backbone atoms of APP (residues 402–417) (Figure 1C). The homology extends to the sidechains constituting the Fe coordinating residues of H-ferritin, E62 and H65, which overlap with potential Fe coordinating residues E412 and E415 of APP695 (Figure 1C).

Recombinant soluble APP695α, representing the predominant neuronal APP species (Rohan de Silva et al., 1997), possessed robust ferroxidase activity (V_{max}= 228.6 μM Fe^{3+}/min/μM

APP; K_m= 48.6 μM; Figure 1D), like Cp (Figure 1E), as measured by the rate of Fe^{3+} incorporation into transferrin. Therefore, APP is a more active ferroxidase than ferritin (V_{max}= 2.21 μM Fe^{3+}/min/μM ferritin, K_m= 200 μM) (Bakker and Boyer, 1986). APP695α ferroxidase activity was maintained across a pH range 5.0–9.0 (Figure S1A). APLP2 was inactive (Figure 2A), like the negative control albumin (Figure S1B), consistent with the absence of the REXXE motif (Figure 1B).

Cp ferroxidase activity is dependent on copper and inhibited by NaN_3 (Osaki, 1966). Neither NaN_3 (Figure 2A) nor Cu^{2+} (2:1 Cu:APP, not shown) altered APP695α activity, indicating that APP695α ferroxidase chemistry is like H-ferritin (Bakker and Boyer, 1986), and not like Cp. H-ferritin ferroxidase activity is inhibited by Zn^{2+} (Bakker and Boyer, 1986) and indeed, Zn^{2+} inhibited the activities of both APP695α and the E2 domain of APP (Figure 2A). Inhibition was specific for Zn^{2+} among physiological divalent metal ions since Ca^{2+} (2 mM), Mg^{2+} (0.5 mM), Cu^{2+} (20 μM), Mn^{2+} (10 μM), Ni^{2+} (20 μM) and Co^{2+} (20 μM), as chloride salts, did not inhibit APP695α ferroxidase activity (not shown). The activities of the main isoforms, APP695α, APP770α, APP751α were identical (Figure S1C).

A 22-residue synthetic peptide within the E2 domain (FD1) (Figure 1A & 2B), containing the putative active site of APP, possessed ferroxidase activity that was ≈ 40% that of APP695α (Figure 2C). Mutational analysis of APP695α (Figure 2A) and FD1 (Figure 2B–D) confirmed that disruption of the REXXE motif, by altering a single conserved amino acid (REWEN, “E14N” in Figure 2B, C), or substituting the homologous pentapeptide regions of APLP1 (REWAM, “EE13/14AM” in Figure 2D) or APLP2 (KEWEE, “R10K” in Figure 2D), abolished activity. Substitution with the homologous H-ferritin sequence (REHAE, “WE12/13HA” in Figure 2B), which does not disrupt the consensus motif, retained activity (Figure 2D).

Like FD1 peptide (Figure 2C), purified E2 polypeptide (Figure 1A) possessed ≈ 40% of the ferroxidase activity of APP695α (Figure 2A). We explored for other domains of APP needed to restore full activity to E2. While purified E1 domain possessed no ferroxidase activity, equimolar concentrations of E1 doubled E2 activity (Figure 2E) to about that of APP695α (Figure 2A). We mapped this potentiation effect to the Growth Factor Domain (GFD) within E1 (Rossjohn et al., 1999) (Figure 2A). GFD did not engender activity from APLP2 (Figure 2A), consistent with the requirement for the REXXE motif.

APP facilitates iron export and interacts with ferroportin

We hypothesized that APP ferroxidase activity may facilitate iron movement analogous to the interaction of Cp with ferroportin (De Domenico et al., 2007). Ferroportin may be expressed in all cells, but Cp is not, leading us to suspect that APP may play the ferroxidase role in certain cells that lack Cp such as HEK293T (De Domenico et al., 2007) and cortical neurons (Klomp et al., 1996). The impact of endogenous APP suppression by RNAi on iron export was therefore initially studied in HEK293T cells, where the absence of Cp was confirmed by western blot (not shown). APP-suppressed cells accumulated significantly more (≈50%, $p<0.01$) radioactive iron (^{59}Fe) than sham RNAi controls (Figure 3A & Figure S2A). Addition of APP695α (2 μM, Figure 3B) or the E2 domain of APP (2 μM, Figure S2A) to the media, after incorporation of ^{59}Fe into the cells, significantly promoted the efflux of ^{59}Fe into the media. E2 lacks the heme-oxygenase (HO) inhibitory domain of APP (Takahashi et al., 2000) (Figure 1A), therefore APP is not promoting iron export in these cells merely through inhibition of HO. Complementary changes in cellular levels of the iron-responsive proteins ferritin and TfR (Figure 3C & D, blots in Figure S2B), consistent with decreased IRP1 & 2 binding to a biotinylated IRE probe (Figure S2C), confirmed that APP acted to lower the LIP. As a further control, we studied the impact of stable transfection of wild-type (WT) or inactive mutant ($FD1^{(E14N)}$-APP695, Figure 2A) APP695 on iron

retention in HEK293T cells. APP695 significantly decreased iron retention compared to cells transfected with vector alone, but FD1$^{(E14N)}$-APP695 increased iron retention, consistent with competition against endogenous APP (Figure S2D-F). These data indicate that ferroxidase-active APP facilitates iron export in HEK293T cells.

Cp co-immunoprecipitates with ferroportin in certain tissues (De Domenico et al., 2007; Jeong and David, 2003). Analogously, most of the ferroportin in HEK293T cells co-immunoprecipitated with endogenous APP (Figure 3E, Figure S2G). Furthermore, the majority of a biotinylated APP695α probe added to HEK293T cells co-immunoprecipitated with ferroportin (Figure 3F), consistent with exogenous APP695α promoting iron export (Figure 3B–D) by interacting with ferroportin.

We next studied iron transport in primary cortical neurons from APP−/− mice. APP−/−; neurons retained significantly more ^{59}Fe than WT neurons (+50%, $p<0.01$) (Figure 4A), and exhibited a corresponding decrease (−60%) in the rate of iron efflux (Figure 4B). The increased retention of iron in APP−/−; neurons was comparable to that reported for Cp−/−; astrocytes over the same 12-hour incubation period (De Domenico et al., 2007; Jeong and David, 2003). APP695α added to WT neurons induced a significant concentration-dependent decrease in ^{59}Fe retention (Figure S3A), and reversed much of the increased ^{59}Fe retention in APP−/−; neurons (Figure 4A). Inactive FD1$^{(E14N)}$-APP695α (Figure 2A), could not promote iron efflux (Figure S3B).

The E2 domain of APP also facilitated iron efflux in primary neuronal cultures (Figure S3C). As with APP-suppressed HEK293T cells (Figure 3C&D), more ferritin and less TfR were detected in APP−/−; compared to WT neurons, exaggerated by the addition of 10 μM iron (Figure 4C, westerns shown in Figure S3D), consistent with increased neuronal iron. We confirmed (Figure S3D) that neocortical neurons do not express Cp (Klomp et al., 1996). Therefore, cortical neurons may depend upon APP as the ferroxidase partner for ferroportin. Consistent with this, APP in human and mouse cortical tissue (including full-length membrane-bound APP) had a major interaction with ferroportin in immunoprecipitation studies (Figure 4D & E, Figure S4A–C). APLP2 did not co-immunoprecipitate with ferroportin from these tissues (Figure 4D).

Neocortical ferroportin also co-immunoprecipitated with Cp (Figure 4D). This was expected, since despite being absent in cortical neurons, Cp is expressed in glia (Klomp et al., 1996). Co-immunoprecipitation of Cp by anti-ferroportin was slightly but significantly increased in APP−/−; brain tissue (Figure S4D & E), possibly due to loss of APP competition for ferroportin interaction. Therefore, ferroportin divides its interactions between APP and Cp in the brain.

However, unlike APP695α (Figs. 3B & 4A), Cp (2 μM) induced no significant increase in ^{59}Fe efflux when added to primary neurons or HEK293T cells (data not shown), consistent with previous observations that the ability of Cp to stabilize ferroportin was cell-type specific and probably limited to cells that express Cp (De Domenico et al., 2007).

Consistent with APP ferroxidase activity being protective, the LD_{50} for Fe^{2+} toxicity was 10-fold higher for primary neurons in culture from WT (2001 μM) compared to APP−/−; mice (234 μM, Figure 4F). However, domains and post-translational modifications outside of the ferroxidase domain, can promote protection against oxidative damage (Furukawa et al., 1996). To appraise the contribution of APP ferroxidase activity to neuroprotection against non-iron oxidative injuries, we studied the effects of APP695 compared to FD1$^{(E14N)}$-APP695 in protecting primary neurons from oxidative stress induced by glutamate excitotoxicity, where sAPPα prevents intracellular Ca^{2+} rise (Furukawa et al., 1996; Mattson et al., 1993). While APP695 significantly prevented glutamate toxicity under

these conditions, the ferroxidase mutant did not (Figure S3E). Although this result raises the hypothesis that some previously reported neuroprotective effects of APP may reflect ferroxidase activity, this is not surprising since the presence of labile iron exacerbates all forms of reactive oxygen species damage (through Fenton chemistry), and therefore the ability of APP ferroxidase domain to minimize labile iron is likely to be protective to some extent against oxidative stress from any origin. We therefore tested whether APP protects the intact brain from toxicity induced by excess iron exposure.

APP prevents iron accumulation and oxidative stress *in vivo*

Aceruloplasminemic patients and Cp knockout mice exhibit marked age-related iron accumulation in liver, pancreas and brain astrocytes (Harris et al., 1995; Patel et al., 2002) but not cortical neurons (Gonzalez-Cuyar et al., 2008; Jeong and David, 2006; Patel et al., 2002). To test whether APP deficiency would cause a similar vulnerability, 12 month old APP−/−; mice were compared to WT age-matched controls fed a normal or high-iron diet for 8 days. Consistent with our cell culture findings (Figures 3 & 4), APP−/−; mice fed a normal diet had significantly more total iron in brain (+26%), liver (+31%), and kidney (+15%) tissue than age-matched controls (Figure 5A; Table S1). After challenge with the high-iron diet, WT mice had no significant change in tissue iron levels. In contrast, APP−/−; mice accumulated significantly more iron in brain (+13%) and particularly liver (+90%) than APP−/−; mice on a normal diet (Figure 5A). Ferritin levels were also increased in brain and liver tissue from APP−/−; mice on the high iron diet (data not shown) consistent with increased iron content. Iron supplementation did not affect the tissue levels of other metals (Table S1).

We examined the livers and cortex of APP−/−; and WT mice with a modified Perl's histological stain, which utilizes intracellular Fe^{2+} to generate H_2O_2 (Gonzalez-Cuyar et al., 2008; Smith et al., 1997). This revealed elevated hepatocytic Fe^{2+} (Figure 5B & E), and intraneuronal Fe^{2+} (Figure 5C, D & F–H) of APP−/−; mice compared to WT matched controls both fed iron. Fe^{2+} accumulation in the brain was confined to neocortical and hippocampal neurons (Figure 5H), while sparing microglia and astrocytes that are known to express Cp (Gonzalez-Cuyar et al., 2008; Harris et al., 1995; Patel et al., 2002). Assay of tissue ferroxidase activity revealed a significant ≈ 40% decrease in APP−/−; brain (Figure 5I). NaN_3-inhibition of Cp activity in WT brain tissue revealed ≈ 40% residual activity, and the complete loss of ferroxidase activity in the brains of APP−/−; mice (Figure 5I). These data are consistent with APP acting as a neuronal ferroxidase. Suppression of APP activity in WT brain tissue with Zn^{2+} revealed ≈ 60% activity consistent with residual Cp ferroxidase activity, and was slightly increased in APP−/−; mice (Figure 5I), perhaps reflecting homeostatic compensation. There were no conspicuous changes in ferroportin or Cp levels in liver and brain samples from APP−/−; mice on a normal or iron-supplemented diet (Figure S4F).

The constitutive abundance of APP in WT liver was found to be similar to that of Cp (Figure S4G). Therefore, the increase in liver iron in APP−/−; mice was consistent with a major loss in the total ferroxidase complement of the tissue. Conversely, APP−/−; heart and lung tissue did not show elevated iron levels even with dietary iron challenge, consistent with these organs having the lowest constitutive levels of APP (Figure S4G) and expressing alternative iron-export ferroxidases, Cp (Figure S4G) and hephaestin (Qian et al., 2007). Similarly, APP levels in astrocytes are much lower than in neurons (Gray and Patel, 1993; Mita et al., 1989; Rohan de Silva et al., 1997), and probably too low to prevent iron accumulation in Cp−/−; astrocytes. Cortical neurons have no redundancy in their export ferroxidases, and therefore accumulate iron in the absence of APP (Figure 5F–H). The likelihood that APP is the unique ferroxidase of cortical neurons is supported by the lack of iron increase in the cortical

neurons of Cp−/−; mice even at an age (24 months) when there is a marked increase in iron in other cells (Jeong and David, 2006; Patel et al., 2002).

Increased Fe^{2+} generates oxidative stress, and indeed the Fe^{2+} increase detected in iron-fed APP−/−; mice was accompanied by increased protein carbonylation (indicative of hydroxyl radical damage, Figure 5J), and decreased glutathione levels (Figure 5K) signifying depleted antioxidant reserves. Despite these signs of stress, stereological counting revealed no significant neuronal loss within the brain in iron-fed mice (data not shown). A more protracted period of iron exposure, or higher doses, may be needed to overcome survival defences. The observation that iron enters the brain neurons of iron-fed APP−/−; mice (Figure 5) also indicates that either APP is a component of the blood-brain barrier, or that prandial iron normally transits the blood-brain barrier to neurons where it is then exported in an APP-dependent manner.

APP ferroxidase activity is inhibited by zinc in AD

We explored whether a failure of APP ferroxidase activity could contribute to the elevated cortical iron that characterizes AD pathology. Elevated iron and ferritin are prominent within the vicinity of amyloid plaques in both humans (Grundke-Iqbal et al., 1990; Lovell et al., 1998; Robinson, 1995) and APP transgenic mice (El Tannir El Tayara et al., 2006; Falangola et al., 2005; Jack et al., 2005). We indeed found a ≈ 45% increase in iron in post-mortem AD cortical tissue (Brodmann area 46), but no change in pathologically-unaffected cerebellum from the same patients (Figure 6A). This matched a 75% ($p<0.001$) decrease in APP ferroxidase activity in the same AD cortical samples compared to the non-demented age-matched samples, with no difference in cerebellar tissue activities (Figure 6B). The ferroxidase activities were confirmed to be APP by immunodepletion experiments (Figure S5A).

The loss of APP ferroxidase activity in AD cortex was not due to decreased levels of APP (Figure S5B). Therefore, a factor in AD cortex appears to inhibit APP. Zn^{2+} is the only identified inhibitor of APP ferroxidase activity (Figure 2A), but total zinc levels were not significantly elevated in the AD cortical samples (Figure S5C). However, Zn^{2+} characteristically accumulates in extracellular amyloid in AD (Lovell et al., 1998; Religa et al., 2006; Suh et al., 2000), which is too small a volume fraction to elevate total tissue zinc levels until the disease is advanced (Religa et al., 2006). Indeed, treatment of the AD cortical samples with the Zn^{2+}-selective chelator TPEN restored APP ferroxidase activity to levels not significantly different from non-demented samples (Figure 6B), confirming that APP is inhibited by Zn^{2+} in AD tissue. TPEN did not significantly change ferroxidase activity in non-demented cortical samples (Figure 6B), indicating that Zn^{2+} is not inhibiting APP in normal tissue. To confirm that the APP ferroxidase activity in AD is being inhibited by Zn^{2+}, we titrated additional Zn^{2+} into samples that had been treated with 20 μM TPEN (Figure S5D). Whereas Zn^{2+} concentrations of ≥ 20 μM were required to suppress APP ferroxidase activity in normal tissue under these conditions, far lower Zn^{2+} concentrations (≥2 μM) suppressed activity in AD samples (IC_{50} for normal tissue = 22.6 μM, IC_{50} for AD =10.2 μM, Figure S5D). Together these data indicate that while there is no clear elevation in total zinc in AD tissue, there is a greater fraction of exchangeable Zn^{2+}, which is inhibiting APP ferroxidase.

Is the Zn^{2+} trapped in extracellular Aβ deposits sufficiently exchangeable to be the source of Zn^{2+} that inhibits APP ferroxidase in AD tissue? To test this we prepared washed (no free Zn^{2+}) synthetic Aβ:Zn^{2+} precipitates, and found that they indeed inhibited APP695α activity as efficiently as free Zn^{2+} in solution, while Aβ alone had no effect (Figure 6C). Therefore, Aβ traps Zn^{2+}, but can readily exchange the Zn^{2+} with APP. Neither free Zn^{2+} nor Aβ:Zn^{2+} complexes inhibited Cp activity (Figure 6C).

Consistent with Aβ presenting Zn^{2+} to suppress APP ferroxidase activity in the brain, there was a significant negative correlation between Aβ burden and APP ferroxidase activity in a series of AD ($p<0.0001$, Figure 6D) and APP transgenic (Tg2576, Figure S5E & F) cortical samples. However, APP ferroxidase activity was not diminished in cortical tissue from Frontal Temporal Dementia or Parkinson's disease (Figure 6E) that lacked amyloid pathology (Table S2), or from Tg2576 mice at an age prior to amyloid pathology (Figure S5E & F).

Discussion

Our findings identify APP as a functional ferroxidase similar to Cp. Both full-length and soluble APP species were found to have major interactions with ferroportin to facilitate iron export from certain cells including neurons (Figure 7). Cp similarly exists in GPI-anchored and soluble forms, with the purpose of separate pools remaining uncertain, although activity at a distance from the cell of origin is likely. While the ferroxidase function of APP is compatible with IRE-regulated translation (Rogers et al., 2002), the relationship between iron-load and APP processing remains to be elucidated, although we note a prior report that exogenous iron promotes α-cleavage in cell culture (Bodovitz et al., 1995). APP therefore plays an important role in preventing iron-mediated oxidative stress through separate domains: a HO-inhibitory domain (Figure 1A) that prevents the release of Fe^{2+} from heme (Takahashi et al., 2000), and, here, a separate ferroxidase domain. The ferroxidase activity of the APP is unique among its protein family, and like ferritin, correlates with the presence of the mRNA IRE motif, which is not present in APLP1 and APLP2 (Figure S6). The ferroxidase center of APP resides in the REXXE consensus motif of the E2 domain, with a remote potentiation domain within the GFD of E1 (Figures 1 & 2). This potentiation by heterologous components is reminiscent of the augmentation of H-ferritin ferroxidase activity by L-ferritin, where the active site is on H-ferritin yet heteropolymers of H and L subunits have a higher ferroxidase activity per H subunit than H homopolymers (Yang et al., 1998).

Cp and APP may be backup ferroxidase activities in tissues where they are colocated (Figure S4E&G) or in glia that express both APP and Cp. The purpose behind such apparent redundancy in some cells is yet unclear. But since neurons lack Cp, APP may be the sole iron-export ferroxidase of neurons. Our findings indicate that inhibition of APP ferroxidase activity may contribute to neuronal iron accumulation in AD cortex. Elevated brain iron is a complication of aging (Bartzokis et al., 1994a; De Domenico et al., 2008; Hallgren and Sourander, 1958; Maynard et al., 2002), and is a feature of several neurodegenerative disorders (Zecca et al., 2004). Failure of ferroxidases Cp (Harris et al., 1995), ferritin (Chinnery et al., 2007) and frataxin (Mantovan et al., 2006) cause various neurodegenerative diseases, and it is intriguing that here another systemically-expressed ferroxidase, APP, is linked to a major brain disease, AD. The elevation of brain iron in AD affects the parenchyma (Bartzokis et al., 1994b; Honda et al., 2005; Smith et al., 1997) but is particularly conspicuous in the dystrophic neurites of amyloid plaques (Grundke-Iqbal et al., 1990; Lovell et al., 1998; Robinson, 1995) where its MRI signal in AD correlates with dementia severity (Ding et al., 2009).

Our data indicate a mechanism by which amyloid pathology could disrupt local iron homeostasis. We found that APP ferroxidase activity is inhibited by a tissue source of Zn^{2+} in AD cortical tissue (Figure 6B). In AD cortex, Aβ binds Zn^{2+} to achieve pathological concentrations (≈1 mM) in plaques (Dong et al., 2003; Lovell et al., 1998; Opazo et al., 2002) and seems a possible reservoir for APP inhibition. Supporting this possibility, Aβ readily transfers Zn^{2+} to inhibit APP ferroxidase activity (Figure 6C), exchangeable Zn^{2+} (as measured by APP inhibition) is increased in AD tissue (Figure S5D), and Aβ burden

inversely correlates with APP ferroxidase activity (Figure 6D). Additionally, Zn^{2+} buffering appears far more limited in AD cortex than non-demented tissue (Figure S5D), which could be consistent with loss of metallothionein III (Uchida et al., 1991) that is released into the synaptic vicinity by astrocytes and prevents metal ion transfer to Aβ (Meloni et al., 2008). Alternatively, oxidation, which is marked in AD tissue, may prevent metallothioneins from binding Zn^{2+} (Hao and Maret, 2005). Since Zn^{2+} induces Aβ aggregation (Bush et al., 1994; Lee et al., 2002), we hypothesize that loss of Zn^{2+} buffering may be an upstream lesion for both amyloid pathology and APP ferroxidase inhibition (Figure 7).

APP is another elevated component of dystrophic neurites within plaque (Cras et al., 1991) where, as noted above, it colocates with high iron concentrations. We hypothesize that in neuritic pathology, elevated iron summons further APP production (Rogers et al., 2002), but the APP generated to export iron becomes inhibited by elevated extracellular Zn^{2+} dissociating from Aβ (Figure 7). This underscores the buffering of Zn^{2+} as a therapeutic strategy for AD, and could explain some activities of Zn^{2+}-ionophores (clioquinol and PBT2) that have shown potent efficacy in preclinical APP transgenic models of AD (Adlard et al., 2008; Cherny et al., 2001) and significantly improved cognition in phase 2 AD clinical trials (Faux et al., 2010; Lannfelt et al., 2008; Ritchie et al., 2003).

The ferroxidase and iron-trafficking properties of APP indicate an important biological activity for a protein whose complex processing has been extensively studied, but which has lacked a conspicuous purpose. These data indicate that some neurotrophic properties of APP and its fragments (Rossjohn et al., 1999) could be mediated by iron regulation.

EXPERIMENTAL PROCEDURES

Human

All human tissue cases were obtained from the Victorian Brain Bank Network. Whole brains are stored at −80°C until required. Cortical tissue from non-demented controls, AD, Parkinson's disease and Frontotemporal dementia were all taken from Brodmann's area 46. Cerebellum tissue was also used from non-demented controls and AD patients. For Aβ analysis, western blots were carried out on total brain homogenates. Ferroxidase activity was tested by transferrin ferroxidase assay on PBS + 1% Triton X-100 (PBST) extracted homogenates.

Biotin labelling of APP695α

Sulfo-NHS-SS-Biotin (Thermo Scientific) was added to APP695α in 20-fold excess and incubated at room temperature for 1 h in phosphate buffered saline (PBS). Removal of non-reacted sulfo-NHS-SS-Biotin was by gel filtration using a Zeba™ Desalt spin column (Thermo Scientific).

Aβ preparation

For aggregation studies, 100μM $A\beta_{1–42}$ was incubated ± 200μM $ZnCl_2$ for 16 h to form precipitates as previously reported (Bush et al., 1994). Insoluble $A\beta_{1–42}$ was then centrifuged at 40,000 g for 10 min and the pellet repeatedly washed in PBS. Aggregated $A\beta_{1–42}$ ± Zn was then added to the Tf ferroxidase assay (described below) at a final concentration of 10 μM $A\beta_{1–42}$ and compared to controls including freshly prepared non-aggregated 10 μM $A\beta_{1–42}$.

Transferrin ferroxidase assay

The assay was based upon established procedures (Bakker and Boyer, 1986), utilizing the spectroscopic change in apo-transferrin when loaded with Fe^{3+}. Km and Vmax values and

curve-fitting were calculated by GraphPad Prism v 5.0. In a cuvette was added (in order): 100 μL ddH_2O, 200 μL HBS buffer (150 mM NaCl, 50 mM HEPES, pH 7.2, 200 μL of 275 μM apo-transferrin, 100 μL of sample (200 nM recombinant protein or 30 μg total tissue homogenate) and 400 μL of 275 μM ferrous ammonium sulfate $(NH_4)_2Fe(SO_4)_2$. For studies of pH-dependence the buffers (50 mM) were: pH 5 sodium acetate, pH 5.5 – 6.5 MES, pH 7.0 – 9.0 Tris. The mixture was incubated for 5 min at 37°C with agitation, and absorbance read at 460 nm. Extinction coefficient of diferric transferrin is 4.56 mM^{-1}.

Immunoprecipitation

HEK293T cells ± 3 h preincubation 2 μM biotin-APP695α, or brain homogenate, was extracted into PBST (or PBS and then sodium carbonate, pH 11 for human brain membrane homogenate), and protein assayed. 100 μg of the sample was then pre-cleared for non-specific binding with protein G agarose beads for 1 h at 4°C. The sample was then incubated with capture antibody (rabbit anti-ferroportin, 1:200, Lifespan Biosciences), mouse anti-N-term APP (22C11), rabbit anti-Cp or mouse anti-APLP2 (1:1000, R&D systems) for 1 h (4°C) before adding fresh equilibrated protein G agarose beads and mixed for a further 2–3 h (4°C). Protein G agarose beads were then washed in PBST and bound proteins were eluted with SDS-PAGE loading buffer. The bound and unbound proteins were separated on 4–20% PAGE (Bis-Tris, Invitrogen) and visualized by western analysis with a detection antibody; mouse anti-N-term APP, mouse anti-Aβ domain of APP (1:500, WO2), rabbit anti-C-term APP (1:10,000, Chemicon), rabbit anti-ferroportin or, in the case of biotin-labelled studies, streptavidin crosslinked to horseradish peroxidase (HRP, 1:15,000, Invitrogen).

Histochemical detection of iron by Perl's staining

For direct visualization of redox- active Fe^{2+} in whole brain hemisphere and liver paraffin embedded sections, a modified Perl's technique was used, as previously described (Gonzalez-Cuyar et al., 2008; Smith et al., 1997). The number of iron positive structures was quantified using colour selection to separate cells from background. Deparaffinized and rehydrated tissue sections (7 μm) were incubated at 37°C for 1 h in 7% potassium ferrocyanide with aqueous hydrochloric acid (3%) and subsequently incubated in 0.75 mg/ml 3,3′-diaminobenzidine and 0.015% H_2O_2 for 5–10 min. When required, sections were counterstaining in Mayer's haematoxylin for 2 min and washed in Scott's tap water before mounting. For brain, the number of iron positive structures was quantified using colour selection to separate cells from background as described in supplemental methods.

Highlights

- APP is a H-ferritin-like ferroxidase, and similarly inhibited by zinc
- APP has a major interaction with ferroportin, facilitating iron export from neurons
- APP−/− mice have elevated hippocampal and cortical neuronal iron and oxidation
- In AD cortex, zinc trapped by accumulated Aβ inhibits APP ferroxidase activity

Supplementary Material

Refer to Web version on PubMed Central for supplementary material.

Acknowledgments

Supported by funds from the National Institute on Aging (1RO1AG12686), the Australian Research Council, the Australian National Health & Medical Research Council (NHMRC), Operational Infrastructure Support Victorian State Government, and the Alzheimer's Association. The Victorian Brain Bank Network is supported by The University of Melbourne, The Mental Health Research Institute, The Alfred Hospital and the Victorian Forensic Institute of Medicine, and funded by Neurosciences Australia and the NHMRC. We thank Gerd Multhaup for helpful comments and for providing APP reagents for pilot studies, Paul Adlard for human tissue samples, and Wilma Wasco for the APLP2 construct.

References

Adlard PA, Cherny RA, Finkelstein DI, Gautier E, Robb E, Cortes M, Volitakis I, Liu X, Smith JP, Perez K, et al. Rapid restoration of cognition in Alzheimer's transgenic mice with 8-hydroxy quinoline analogs is associated with decreased interstitial Abeta. Neuron. 2008; 59:43–55. [PubMed: 18614028]

Bakker GR, Boyer RF. Iron incorporation into apoferritin. The role of apoferritin as a ferroxidase. J Biol Chem. 1986; 261:13182–13185. [PubMed: 3759957]

Bartzokis G, Mintz J, Sultzer D, Marx P, Herzberg JS, Phelan CK, Marder SR. In vivo MR evaluation of age-related increases in brain iron. AJNR Am J Neuroradiol. 1994a; 15:1129–1138. [PubMed: 8073983]

Bartzokis G, Sultzer D, Mintz J, Holt LE, Marx P, Phelan CK, Marder SR. In vivo evaluation of brain iron in Alzheimer's disease and normal subjects using MRI. Biol Psychiatry. 1994b; 35:480–487. [PubMed: 8018799]

Bartzokis G, Tishler TA. MRI evaluation of basal ganglia ferritin iron and neurotoxicity in Alzheimer's and Huntingon's disease. Cell Mol Biol (Noisy-le-grand). 2000; 46:821–833. [PubMed: 10875443]

Bodovitz S, Falduto MT, Frail DE, Klein WL. Iron levels modulate alpha-secretase cleavage of amyloid precursor protein. J Neurochem. 1995; 64:307–315. [PubMed: 7798927]

Bush AI, Pettingell WH, Multhaup G, d Paradis M, Vonsattel JP, Gusella JF, Beyreuther K, Masters CL, Tanzi RE. Rapid induction of Alzheimer A beta amyloid formation by zinc. Science. 1994; 265:1464–1467. [PubMed: 8073293]

Cherny RA, Atwood CS, Xilinas ME, Gray DN, Jones WD, McLean CA, Barnham KJ, Volitakis I, Fraser FW, Kim Y, et al. Treatment with a copper-zinc chelator markedly and rapidly inhibits beta-amyloid accumulation in Alzheimer's disease transgenic mice. Neuron. 2001; 30:665–676. [PubMed: 11430801]

Cherny RA, Legg JT, McLean CA, Fairlie D, Huang X, Atwood CS, Beyreuther K, Tanzi RE, Masters CL, Bush AI. Aqueous dissolution of Alzheimer's disease Aβ amyloid deposits by biometal depletion. Journal of Biological Chemistry. 1999; 274:23223–23228. [PubMed: 10438495]

Chinnery PF, Crompton DE, Birchall D, Jackson MJ, Coulthard A, Lombes A, Quinn N, Wills A, Fletcher N, Mottershead JP, et al. Clinical features and natural history of neuroferritinopathy caused by the FTL1 460InsA mutation. Brain. 2007; 130:110–119. [PubMed: 17142829]

Cras P, Kawai M, Lowery D, Gonzalez-DeWhitt P, Greenberg B, Perry G. Senile plaque neurites in Alzheimer disease accumulate amyloid precursor protein. Proc Natl Acad Sci U S A. 1991; 88:7552–7556. [PubMed: 1652752]

De Domenico I, Nemeth E, Nelson JM, Phillips JD, Ajioka RS, Kay MS, Kushner JP, Ganz T, Ward DM, Kaplan J. The hepcidin-binding site on ferroportin is evolutionarily conserved. Cell Metab. 2008; 8:146–156. [PubMed: 18680715]

De Domenico I, Ward DM, di Patti MC, Jeong SY, David S, Musci G, Kaplan J. Ferroxidase activity is required for the stability of cell surface ferroportin in cells expressing GPI-ceruloplasmin. EMBO J. 2007; 26:2823–2831. [PubMed: 17541408]

Ding B, Chen KM, Ling HW, Sun F, Li X, Wan T, Chai WM, Zhang H, Zhan Y, Guan YJ. Correlation of iron in the hippocampus with MMSE in patients with Alzheimer's disease. J Magn Reson Imaging. 2009; 29:793–798. [PubMed: 19306401]

Dong J, Atwood CS, Anderson VE, Siedlak SL, Smith MA, Perry G, Carey PR. Metal binding and oxidation of amyloid-beta within isolated senile plaque cores: Raman microscopic evidence. Biochemistry. 2003; 42:2768–2773. [PubMed: 12627941]

El Tannir El Tayara N, Delatour B, Le Cudennec C, Guegan M, Volk A, Dhenain M. Age-related evolution of amyloid burden, iron load, and MR relaxation times in a transgenic mouse model of Alzheimer's disease. Neurobiol Dis. 2006; 22:199–208. [PubMed: 16337798]

Falangola MF, Lee SP, Nixon RA, Duff K, Helpern JA. Histological co-localization of iron in Abeta plaques of PS/APP transgenic mice. Neurochem Res. 2005; 30:201–205. [PubMed: 15895823]

Faux NG, Ritchie CW, Gunn A, Rembach A, Tsatsanis A, Bedo J, Harrison J, Lannfelt L, Blennow K, Zetterberg H, et al. PBT2 Rapidly Improves Cognition in Alzheimer's Disease: Additional Phase II Analyses. J Alzheimers Dis. 2010; 20:509–516. [PubMed: 20164561]

Furukawa K, Sopher BL, Rydel RE, Begley JG, Pham DG, Martin GM, Fox M, Mattson MP. Increased activity-regulating and neuroprotective efficacy of alpha-secretase-derived secreted amyloid precursor protein conferred by a C-terminal heparin-binding domain. J Neurochem. 1996; 67:1882–1896. [PubMed: 8863493]

Gonzalez-Cuyar LF, Perry G, Miyajima H, Atwood CS, Riveros-Angel M, Lyons PF, Siedlak SL, Smith MA, Castellani RJ. Redox active iron accumulation in aceruloplasminemia. Neuropathology. 2008; 28:466–471. [PubMed: 18282164]

Gray CW, Patel AJ. Induction of beta-amyloid precursor protein isoform mRNAs by bFGF in astrocytes. Neuroreport. 1993; 4:811–814. [PubMed: 8347831]

Grundke-Iqbal I, Fleming J, Tung YC, Lassmann H, Iqbal K, Joshi JG. Ferritin is a component of the neuritic (senile) plaque in Alzheimer dementia. Acta Neuropathol. 1990; 81:105–110. [PubMed: 2082650]

Gutierrez JA, Yu J, Rivera S, Wessling-Resnick M. Functional expression cloning and characterization of SFT, a stimulator of Fe transport. J Cell Biol. 1997; 139:895–905. [PubMed: 9362508]

Hallgren B, Sourander P. The effect of age on the non-haemin iron in the human brain. J Neurochem. 1958; 3:41–51. [PubMed: 13611557]

Hao Q, Maret W. Imbalance between pro-oxidant and pro-antioxidant functions of zinc in disease. J Alzheimers Dis. 2005; 8:161–170. discussion 209–115. [PubMed: 16308485]

Harris ZL, Takahashi Y, Miyajima H, Serizawa M, MacGillivray RT, Gitlin JD. Aceruloplasminemia: molecular characterization of this disorder of iron metabolism. Proc Natl Acad Sci U S A. 1995; 92:2539–2543. [PubMed: 7708681]

Honda K, Smith MA, Zhu X, Baus D, Merrick WC, Tartakoff AM, Hattier T, Harris PL, Siedlak SL, Fujioka H, et al. Ribosomal RNA in Alzheimer disease is oxidized by bound redox-active iron. J Biol Chem. 2005; 280:20978–20986. [PubMed: 15767256]

Jack CR Jr, Wengenack TM, Reyes DA, Garwood M, Curran GL, Borowski BJ, Lin J, Preboske GM, Holasek SS, Adriany G, et al. In vivo magnetic resonance microimaging of individual amyloid plaques in Alzheimer's transgenic mice. J Neurosci. 2005; 25:10041–10048. [PubMed: 16251453]

Jeong SY, David S. Glycosylphosphatidylinositol-anchored ceruloplasmin is required for iron efflux from cells in the central nervous system. J Biol Chem. 2003; 278:27144–27148. [PubMed: 12743117]

Jeong SY, David S. Age-related changes in iron homeostasis and cell death in the cerebellum of ceruloplasmin-deficient mice. J Neurosci. 2006; 26:9810–9819. [PubMed: 16988052]

Klausner RD, Rouault TA, Harford JB. Regulating the fate of mRNA: the control of cellular iron metabolism. Cell. 1993; 72:19–28. [PubMed: 8380757]

Klomp LW, Farhangrazi ZS, Dugan LL, Gitlin JD. Ceruloplasmin gene expression in the murine central nervous system. J Clin Invest. 1996; 98:207–215. [PubMed: 8690795]

Lannfelt L, Blennow K, Zetterberg H, Batsman S, Ames D, Harrison J, Masters CL, Targum S, Bush AI, Murdoch R, et al. Safety, efficacy, and biomarker findings of PBT2 in targeting Abeta as a modifying therapy for Alzheimer's disease: a phase IIa, double-blind, randomised, placebo-controlled trial. Lancet Neurol. 2008; 7:779–786. [PubMed: 18672400]

Lawson DM, Artymiuk PJ, Yewdall SJ, Smith JM, Livingstone JC, Treffry A, Luzzago A, Levi S, Arosio P, Cesareni G, et al. Solving the structure of human H ferritin by genetically engineering intermolecular crystal contacts. Nature. 1991; 349:541–544. [PubMed: 1992356]

Lawson DM, Treffry A, Artymiuk PJ, Harrison PM, Yewdall SJ, Luzzago A, Cesareni G, Levi S, Arosio P. Identification of the ferroxidase centre in ferritin. FEBS Lett. 1989; 254:207–210. [PubMed: 2776883]

Lee JY, Cole TB, Palmiter RD, Suh SW, Koh JY. Contribution by synaptic zinc to the gender-disparate plaque formation in human Swedish mutant APP transgenic mice. Proc Natl Acad Sci U S A. 2002; 99:7705–7710. [PubMed: 12032347]

Lovell MA, Robertson JD, Teesdale WJ, Campbell JL, Markesbery WR. Copper, iron and zinc in Alzheimer's disease senile plaques. J Neurol Sci. 1998; 158:47–52. [PubMed: 9667777]

Mantovan MC, Martinuzzi A, Squarzanti F, Bolla A, Silvestri I, Liessi G, Macchi C, Ruzza G, Trevisan CP, Angelini C. Exploring mental status in Friedreich's ataxia: a combined neuropsychological, behavioral and neuroimaging study. Eur J Neurol. 2006; 13:827–835. [PubMed: 16879292]

Mattson MP, Cheng B, Culwell AR, Esch FS, Lieberburg I, Rydel RE. Evidence for excitoprotective and intraneuronal calcium-regulating roles for secreted forms of the β-amyloid precursor protein. Neuron. 1993; 10:243–254. [PubMed: 8094963]

Maynard CJ, Cappai R, Volitakis I, Cherny RA, White AR, Beyreuther K, Masters CL, Bush AI, Li QX. Overexpression of Alzheimer's disease amyloid-beta opposes the age-dependent elevations of brain copper and iron. J Biol Chem. 2002; 277:44670–44676. [PubMed: 12215434]

Meloni G, Sonois V, Delaine T, Guilloreau L, Gillet A, Teissie J, Faller P, Vasak M. Metal swap between Zn7-metallothionein-3 and amyloid-beta-Cu protects against amyloid-beta toxicity. Nat Chem Biol. 2008; 4:366–372. [PubMed: 18454142]

Miller LM, Wang Q, Telivala TP, Smith RJ, Lanzirotti A, Miklossy J. Synchrotron-based infrared and X-ray imaging shows focalized accumulation of Cu and Zn co-localized with beta-amyloid deposits in Alzheimer's disease. Journal of structural biology. 2006; 155:30–37. [PubMed: 16325427]

Mita S, Schon EA, Herbert J. Widespread expression of amyloid beta-protein precursor gene in rat brain. Am J Pathol. 1989; 134:1253–1261. [PubMed: 2502926]

Ninomiya H, Roch JM, Sundsmo MP, Otero DA, Saitoh T. Amino acid sequence RERMS represents the active domain of amyloid beta/A4 protein precursor that promotes fibroblast growth. J Cell Biol. 1993; 121:879–886. [PubMed: 8491779]

Opazo C, Huang X, Cherny R, Moir R, Roher A, White A, Cappai R, Masters C, Tanzi R, Inestrosa N, et al. Metalloenzyme-like activity of Alzheimer's disease β-amyloid: Cu-dependent catalytic conversion of dopamine, cholesterol and biological reducing agents to neurotoxic H_2O_2. Journal of Biological Chemistry. 2002; 277:40302–40308. [PubMed: 12192006]

Osaki S. Kinetic studies of ferrous ion oxidation with crystalline human ferroxidase (ceruloplasmin). J Biol Chem. 1966; 241:5053–5059. [PubMed: 5925868]

Patel BN, Dunn RJ, Jeong SY, Zhu Q, Julien JP, David S. Ceruloplasmin regulates iron levels in the CNS and prevents free radical injury. J Neurosci. 2002; 22:6578–6586. [PubMed: 12151537]

Qian ZM, Chang YZ, Leung G, Du JR, Zhu L, Wang Q, Niu L, Xu YJ, Yang L, Ho KP, et al. Expression of ferroportin1, hephaestin and ceruloplasmin in rat heart. Biochim Biophys Acta. 2007; 1772:527–532. [PubMed: 17383861]

Religa D, Strozyk D, Cherny RA, Volitakis I, Haroutunian V, Winblad B, Naslund J, Bush AI. Elevated cortical zinc in Alzheimer disease. Neurology. 2006; 67:69–75. [PubMed: 16832080]

Ritchie CW, Bush AI, Mackinnon A, Macfarlane S, Mastwyk M, MacGregor L, Kiers L, Cherny R, Li QX, Tammer A, et al. Metal-protein attenuation with iodochlorhydroxyquin (clioquinol) targeting Abeta amyloid deposition and toxicity in Alzheimer disease: a pilot phase 2 clinical trial. Arch Neurol. 2003; 60:1685–1691. [PubMed: 14676042]

Robinson SR, Noone DF, Kril J, Halliday GM. Most amyloid plaques contain ferritin-rich cells. Alzheimer's Research. 1995; 1:191–196.

Rogers JT, Randall JD, Cahill CM, Eder PS, Huang X, Gunshin H, Leiter L, McPhee J, Sarang SS, Utsuki T, et al. An iron-responsive element type II in the 5′-untranslated region of the Alzheimer's amyloid precursor protein transcript. J Biol Chem. 2002; 277:45518–45528. [PubMed: 12198135]

Rohan de Silva HA, Jen A, Wickenden C, Jen LS, Wilkinson SL, Patel AJ. Cell-specific expression of beta-amyloid precursor protein isoform mRNAs and proteins in neurons and astrocytes. Brain Res Mol Brain Res. 1997; 47:147–156. [PubMed: 9221912]

Rossjohn J, Cappai R, Feil SC, Henry A, McKinstry WJ, Galatis D, Hesse L, Multhaup G, Beyreuther K, Masters CL, et al. Crystal structure of the N-terminal, growth factor-like domain of Alzheimer amyloid precursor protein. Nat Struct Biol. 1999; 6:327–331. [PubMed: 10201399]

Smith MA, Harris PL, Sayre LM, Perry G. Iron accumulation in Alzheimer disease is a source of redox-generated free radicals. Proc Natl Acad Sci U S A. 1997; 94:9866–9868. [PubMed: 9275217]

Suh SW, Jensen KB, Jensen MS, Silva DS, Kesslak PJ, Danscher G, Frederickson CJ. Histochemically-reactive zinc in amyloid plaques, angiopathy, and degenerating neurons of Alzheimer's diseased brains. Brain Res. 2000; 852:274–278. [PubMed: 10678753]

Takahashi M, Dore S, Ferris CD, Tomita T, Sawa A, Wolosker H, Borchelt DR, Iwatsubo T, Kim SH, Thinakaran G, et al. Amyloid precursor proteins inhibit heme oxygenase activity and augment neurotoxicity in Alzheimer's disease. Neuron. 2000; 28:461–473. [PubMed: 11144356]

Toussaint L, Bertrand L, Hue L, Crichton RR, Declercq JP. High-resolution X-ray structures of human apoferritin H-chain mutants correlated with their activity and metal-binding sites. J Mol Biol. 2007; 365:440–452. [PubMed: 17070541]

Uchida Y, Takio K, Titani K, Ihara Y, Tomonaga M. The growth-inhibitory factor that is deficient in the Alzheimer's disease brain is a 68-amino acid metallothionein-like protein. Neuron. 1991; 7:337–347. [PubMed: 1873033]

Visser CC, Voorwinden LH, Crommelin DJ, Danhof M, de Boer AG. Characterization and modulation of the transferrin receptor on brain capillary endothelial cells. Pharm Res. 2004; 21:761–769. [PubMed: 15180331]

Wang Y, Ha Y. The X-ray structure of an antiparallel dimer of the human amyloid precursor protein E2 domain. Mol Cell. 2004; 15:343–353. [PubMed: 15304215]

Yamamoto A, Shin RW, Hasegawa K, Naiki H, Sato H, Yoshimasu F, Kitamoto T. Iron (III) induces aggregation of hyperphosphorylated tau and its reduction to iron (II) reverses the aggregation: implications in the formation of neurofibrillary tangles of Alzheimer's disease. J Neurochem. 2002; 82:1137–1147. [PubMed: 12358761]

Yang X, Chen-Barrett Y, Arosio P, Chasteen ND. Reaction paths of iron oxidation and hydrolysis in horse spleen and recombinant human ferritins. Biochemistry. 1998; 37:9743–9750. [PubMed: 9657687]

Zecca L, Youdim MB, Riederer P, Connor JR, Crichton RR. Iron, brain ageing and neurodegenerative disorders. Nat Rev Neurosci. 2004; 5:863–873. [PubMed: 15496864]

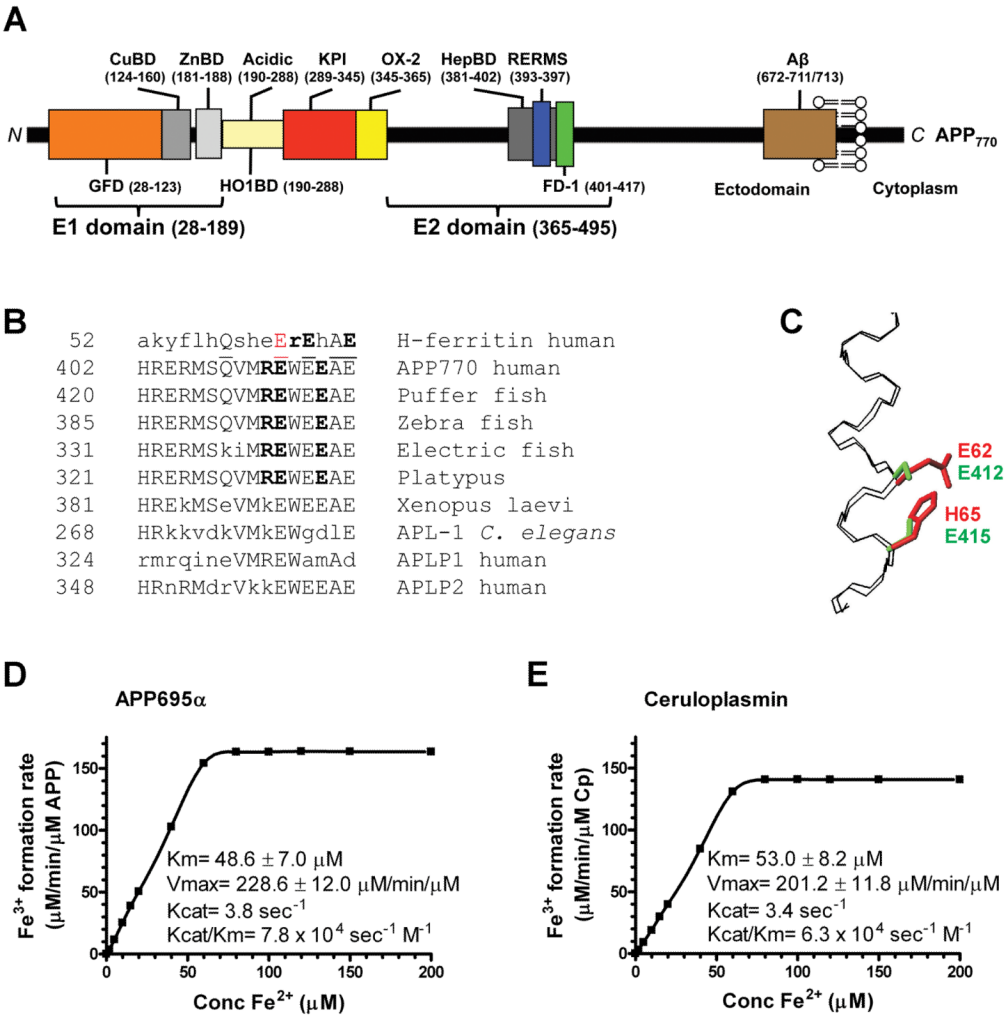

Figure 1. Characterization of APP695α ferroxidase activity

A, Schematic of APP domains. The APP_{770} isoform is shown, APP_{751} lacks the OX-2 domain, and APP_{695} lacks both OX-2 and Kunitz protease inhibitor (KPI) domains. CuBD= copper binding domain, ZnBD= zinc binding domain. **B,** Sequence homologies for the REXXE motif. A sole match for the REXXE motif (in bold) of H-ferritin is at residues 411–415 of human APP770, commencing 5 residues downstream from the RERMS neurotrophic motif (Ninomiya et al., 1993). This is an evolutionarily-conserved motif not present in either human APLP1 or APLP2. A consensus alignment of three glutamate residues and the ferroxidase active site of H-ferritin is underlined. The first glutamate of the REWEE motif of APP could be aligned with Glu62 of H-ferritin (in red), which is part of the ferroxidase catalytic site (Lawson et al., 1989; Toussaint et al., 2007) although this forces the REXXE motifs of the proteins two residues out of register. **C**, An overlay of the backbone atoms (N, Cα, C) of residues 52–67 of the known H-ferritin active site (Lawson et al., 1991) (PDB accession no. 1FHA) with the putative ferroxidase site within residues 402–417 of APP695 (Wang and Ha, 2004) (1rw6) (RMSD 0.4 Å). The Fe coordinating residues of H-ferritin, E62 and H65 (shown in red) overlap with the corresponding residues E412 and E415 that make up the putative ferroxidase site of APP (shown in green), based upon the sequence alignment in **C. D & E,** Kinetic values of Fe^{3+} formation from Fe^{2+} monitored by incorporation into transferrin, indicated within the graphs, were calculated for each protein

(200 nM) incubated with various concentrations of Fe^{2+} at pH 7.2 to reflect the normal pH of brain interstitial space, where apo-transferrin is abundant (Visser et al., 2004). Cp values are in close agreement with the original reports (Osaki, 1966). Data are means± SEM, n= 3 replicates, typical of 3 experiments. See also Figure S1.

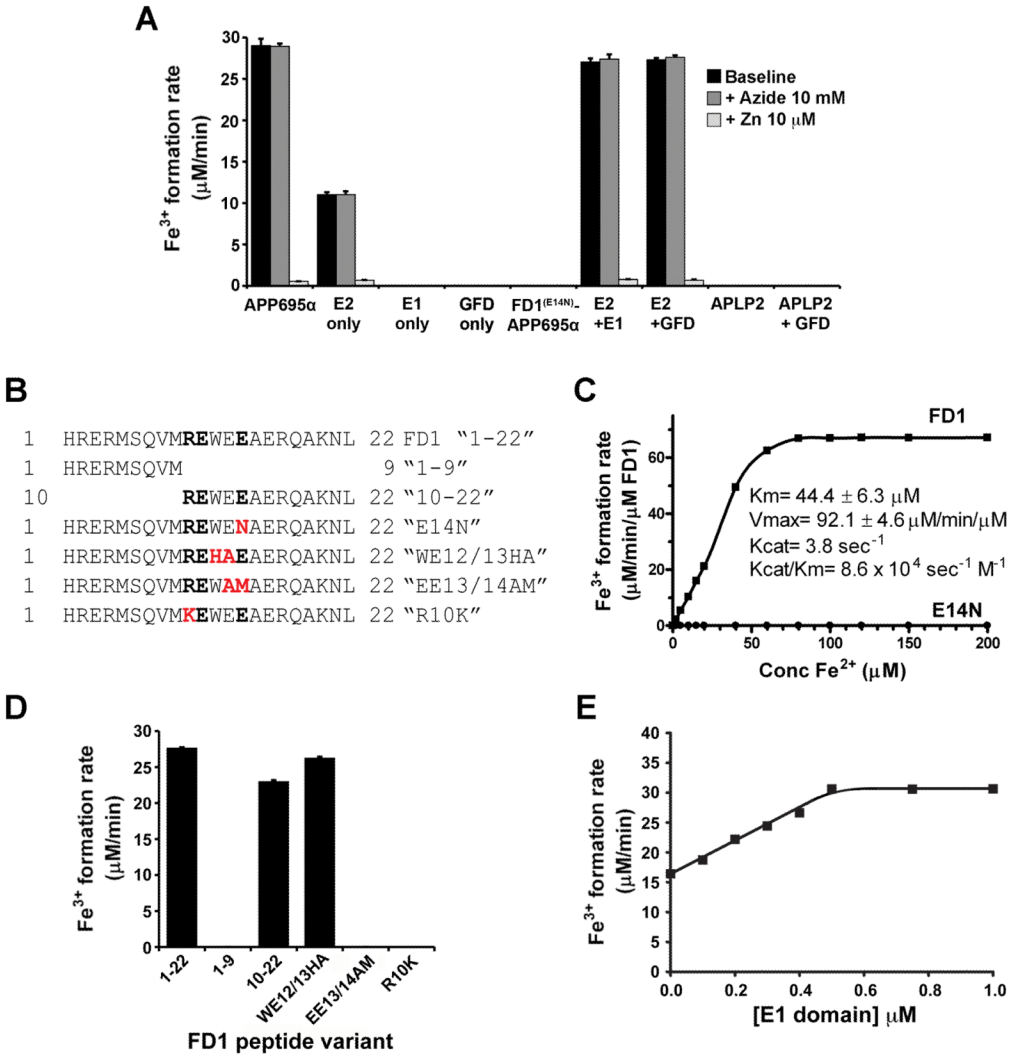

Figure 2. Domains important to APP ferroxidase activity and its inhibition by Zn^{2+}

A, Activities of the E2 fragment of APP ± GFD-containing fragments compared to APP695α FD1$^{(E14N)}$-APPα and APLP2α in HBS, pH7.2. Effects of ferroxidase inhibitors NaN_3 (10 mM) for Cp, and Zn^{2+} (10 μM) for H-ferritin, are shown. FD1$^{(E14N)}$-APP695α has the mutation in the REXXE motif shown in Figure 2B, C. **B,** Sequences of FD1 and derived peptides used to map the active site of APP695α. The REXXE motif is in bold, and the substitution site in red. The last 3 peptides have substitutions in the putative active site that represent the homologous sequences of H-ferritin, APLP1 and APLP2, respectively. **C,** Ferroxidase activities of a 22-residue peptide containing the REXXE consensus motif of APP ("FD1", see **B**) and the same peptide where the REWEE sequence is substituted with REWEN ("E14N", see **B**). **D,** Ferroxidase activity of FD1 is specific to the REXXE motif. Activity is retained upon deleting the first 9 residues (containing the RERMS motif), and when the H-ferritin REXXE consensus motif is substituted into the peptide (WE12/13HA). Activity is eliminated by substitution of the APLP1 (EE13/14AM) and APLP2 (R10K) sequence, which disrupt the REXXE consensus sequence. All peptides were 0.5 μM. **E,** Ferroxidase activity of the E2 domain of APP (0.5 μM) is potentiated by the E1 domain in a concentration-dependent manner up to a 1:1 stoichiometry. Values are means ± SEM, n= 3 replicates, typical of 3 experiments. See also Figure S1.

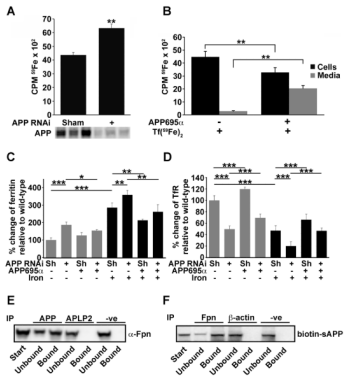

Figure 3. APP promotes iron release, lowers the labile iron pool and interacts with ferroportin in HEK293T cells

A, Iron flux was measured after incorporation of $Tf(^{59}Fe)_2$. APP RNAi (vs non-specific scrambled RNAi, "sham") induces cellular ^{59}Fe retention. Suppression of APP, in triplicate, was confirmed by western blot (22C11). **B,** APP695α (2 μM) added to the media promotes ^{59}Fe export over 6h. **C & D,** Western blot (as shown in Figure S2B) quantification: APP RNAi increased ferritin (to ≈ 200%) and decreased TfR levels (to ≈ 50%), while APP695α partially reversed these effects. Additional iron ($Fe(NH_4)_2(SO_4)_2$,10 μM) raised the baseline ferritin and lowered the TfR, but the effect of adding or subtracting APP was similar. Sh = "sham", non-specific scrambled RNAi. **E**, Interaction of APP with ferroportin using anti-Fpn for detection and anti-N-terminal APP for immunoprecipitation of HEK293T cells treated with iron (10 μM). No interaction with APLP2 confirmed specificity to APP. Non-specific rabbit IgG was used as a control ("-ve"). **F**, Biotin-labelled APP695α, when added to the media of HEK293T cells treated with $Fe(NH_4)_2(SO_4)_2$ (10 μM), is immunoprecipitated from the cell homogenate with anti-Fpn antibody. Data are means ± SEM of n=3. *= $p<0.05$, **= $p<0.01$, ***= $p<0.001$; A & B analysed by 2-tailed t-tests, C & D by ANOVA + Dunnet's tests. See also Figure S2.

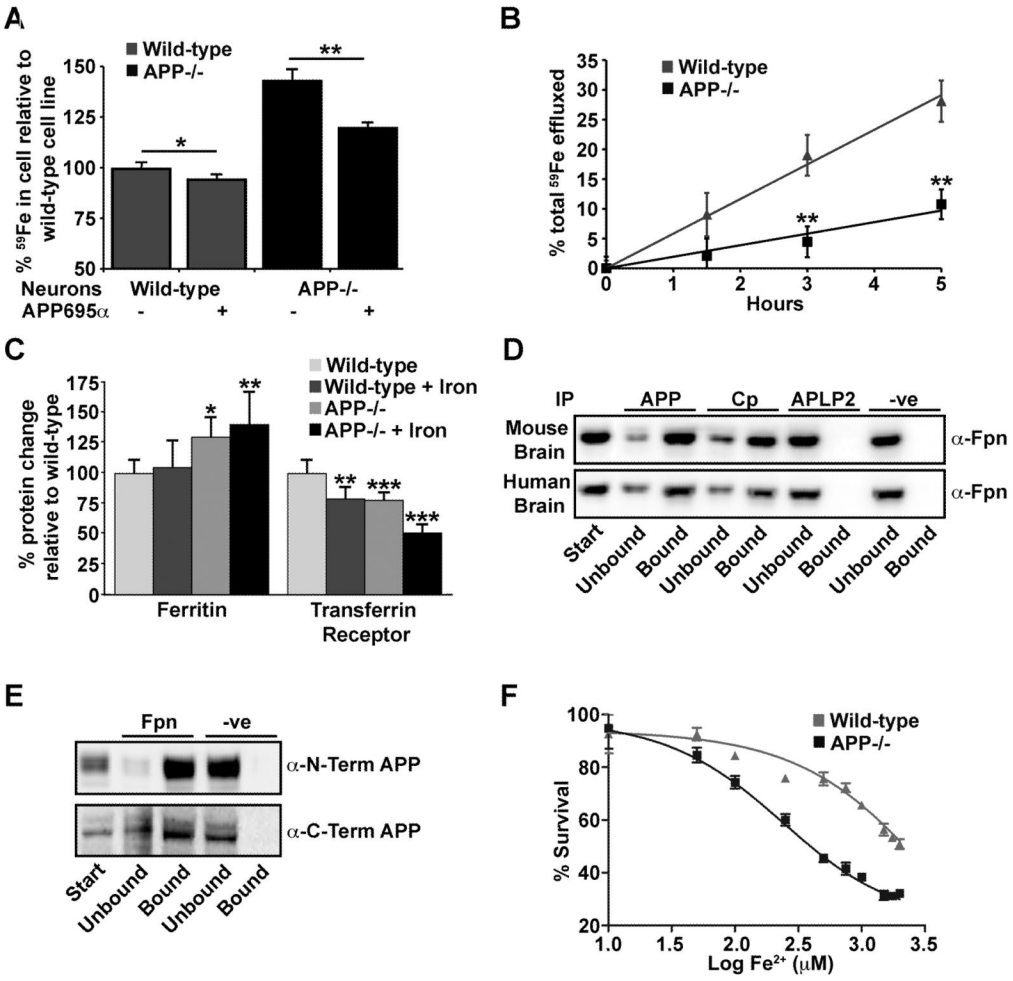

Figure 4. Intracellular iron accumulates in APP−/− neurons

A, APP−/−; primary neurons treated with Tf(^{59}Fe)$_2$ retain more ^{59}Fe after 12 h than cells from WT controls. APP695α (2 μM) promotes ^{59}Fe export into the media after 12 h from both WT and APP−/−; neurons. In APP−/−; neurons this reduces intracellular iron to approach WT levels. **B,** ^{59}Fe media efflux is decreased for APP−/−; compared to WT primary neurons. Data are ^{59}Fe counts in media expressed as a fraction of the total in culture. **C,** Western blot (see Figure S3D) quantification of ferritin and TfR in primary neuronal cultures from WT and APP−/−; matched controls treated ± $Fe(NH_4)_2(SO_4)_2$ (75 μM). Differences in APP−/−; cells are consistent with increased retention of iron. **D,** APP and Cp co-immunoprecipitate with ferroportin from human and mouse brain, but not APLP2. **E**, Determination that membrane-bound full-length APP interacts with ferroportin using APP detection antibodies for both the N- and C-terminal ends of the protein from membrane lysate of human brain immunoprecipitated by anti-Fpn antibody. **F,** APP−/−; neurons incubated with increasing concentrations of $Fe(NH_4)_2(SO_4)_2$ are more susceptible to iron toxicity, measured by CCK-8 cell viability assay, than WT neurons. Data are means ± SEM, n=3, *= p<0.05, **= p<0.01, ***= p<0.001, **A - C** analysed by 2-tailed t- tests, **D** by ANOVA + Dunnet's test compared to WT. See also Figures S3 and S4.

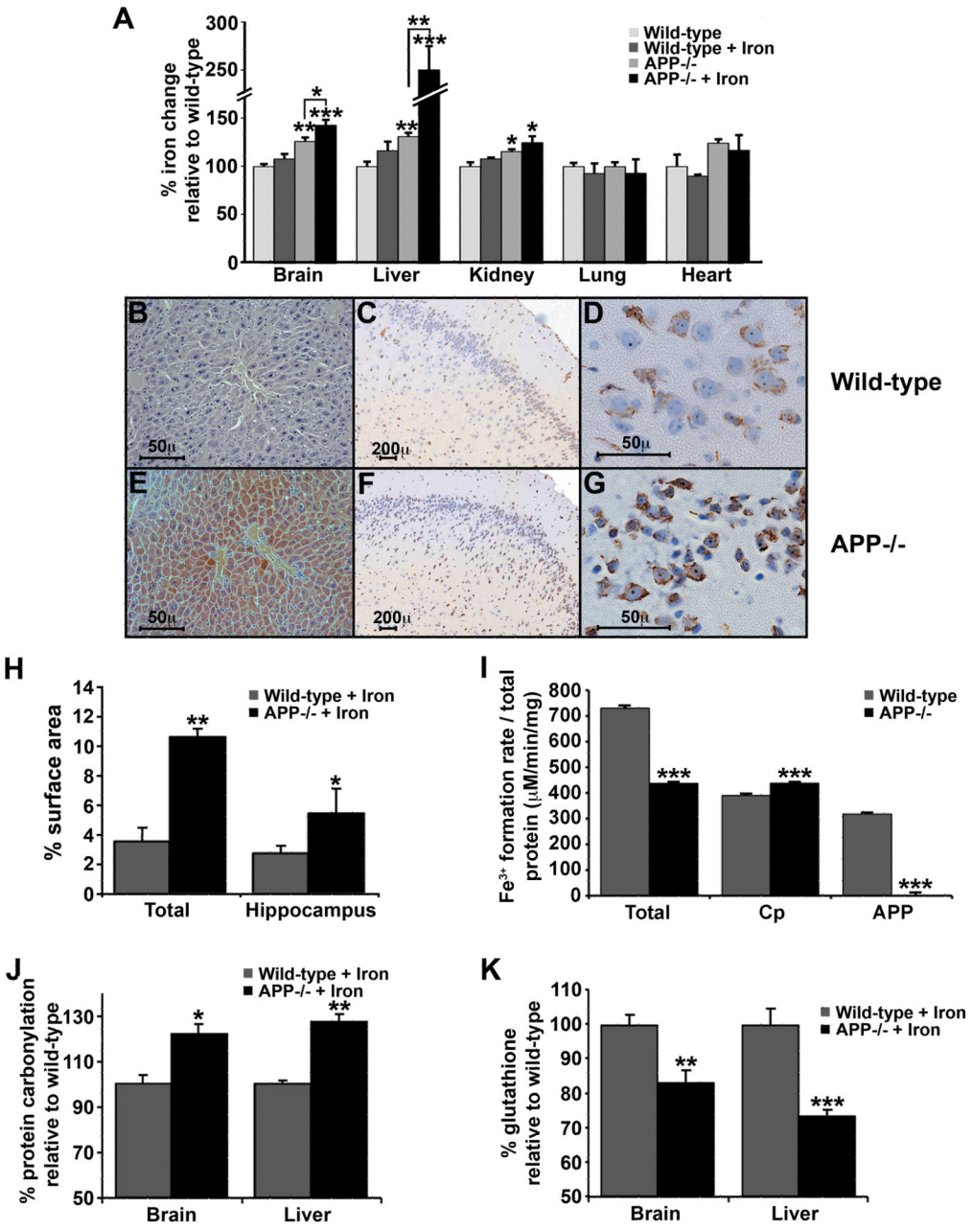

Figure 5. Dietary iron challenge increases tissue iron in APP−/− but not normal mice

A, 12 month old APP−/−; mice accumulate iron within brain (≈125%), liver (≈130%) and kidney (≈115%) tissue compared to WT matched controls. Iron levels were further increased in brain (≈140%) and liver (≈250%) of APP−/−; mice fed a high iron diet for 8 days, which did not alter iron levels in WT matched controls. **B–G,** Labile redox-active iron detected by modified Perl's staining in hepatocytes (**B, E**) and cortical neurons (**C–D & F–G**) from APP−/−; (**E–G**) and WT matched controls (**B–D**) fed a high iron diet. **H,** Computer-assisted quantification of modified Perl's-stained surface area of brain sections from mice fed on a high iron diet (n=4 mice, average of 3 sections each), indicates that APP −/−; mice have significantly more redox-active iron positive cells per hemisphere, and in the hippocampus, compared to WT. **I,** Ferroxidase activity in brain from APP−/−; mice is

decreased compared to WT matched controls. Cp activity is determined after treatment of the tissue with Zn^{2+} to inhibit the activity of APP. APP activity is determined after treatment of the tissue with NaN_3 to inhibit the activity of Cp. **J–K**, In accord with increased redox-active iron in liver and brain from APP−/−; mice, significantly increased protein carbonylation occurs in APP−/−; mice fed on a high iron diet (**J**) and decreased glutathione in APP−/−; ± high iron diet (**K**). Data are means ± SEM, n=4, *= $p<0.05$, **= $p<0.01$, ***= $p<0.001$, A analysed by ANOVA + Dunnet's test compared to WT, H-K by 2-tailed t-tests. See also Figure S4 and Table S1.

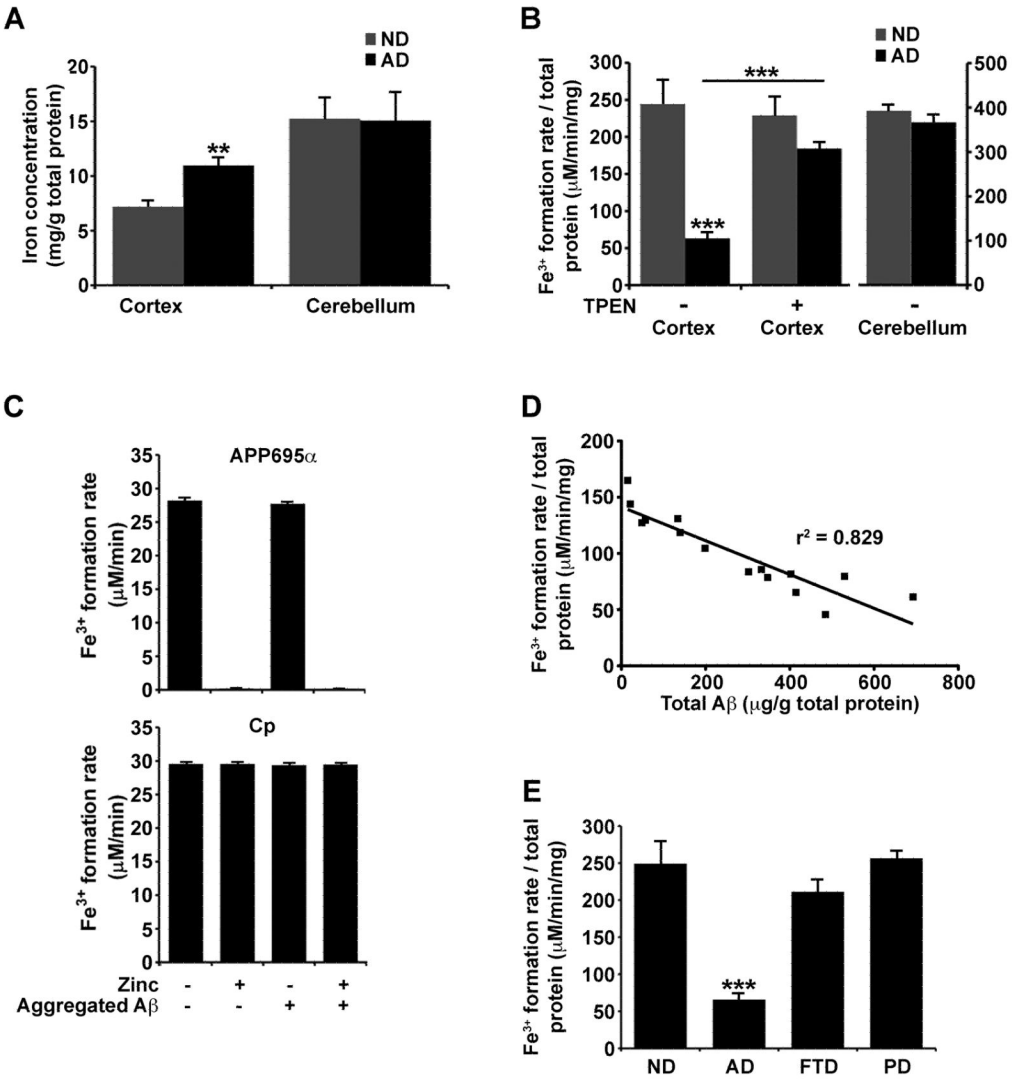

Figure 6. Decreased cortical APP ferroxidase activity in Alzheimer's Disease

A, AD cortical tissue accumulates iron compared to age-matched non-demented (ND) samples. Iron levels were not changed in pathologically unaffected cerebellum from the same subjects. **B,** APP-specific ferroxidase activity is decreased in AD cortical tissue (≈75%) but not in cerebellum, consistent with the pattern of iron accumulation in **A**. Chelating Zn^{2+} from the tissue with TPEN restores the APP ferroxidase activity in AD sample to levels comparable to ND cortex. **C,** Both free Zn^{2+}, as well as Zn^{2+} dissociating from washed Zn^{2+}:$A\beta_{1-42}$ aggregates, inhibit APP695α ferroxidase activity but not Cp activity. **D**, Decrease in APP-specific ferroxidase activity correlates with increased Aβ content in AD cortical tissue ($p<0.0001$, $r^2= 0.829$). **E**, APP ferroxidase activity is not changed in cortical tissue from non-β-amyloid burdened neurodegenerative diseases such as frontotemporal dementia and Parkinson's disease. **A–C & E**, Data are means ±SEM, n=8, **= $p<0.01$, ***= $p<0.001$ by 2-tailed t-tests. See also Figure S1. See also Figure S5 and Table S2.

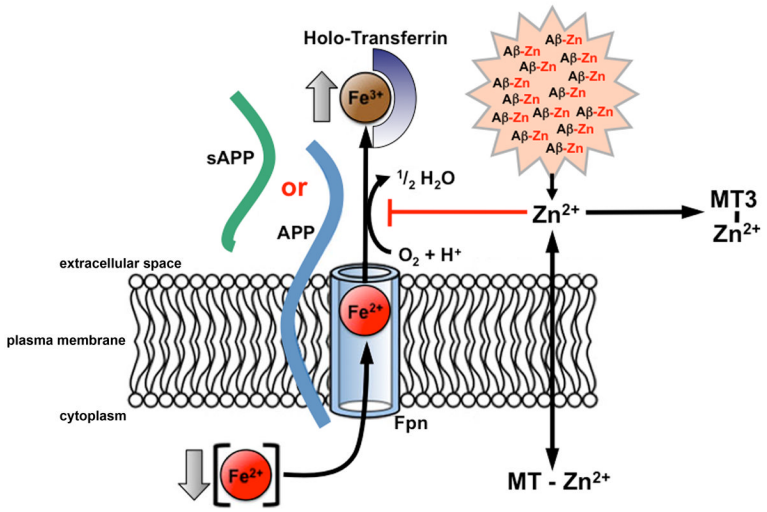

Figure 7. Model for the role of APP in cellular iron export and its inhibition in Alzheimer's disease

Fpn transports Fe^{2+} from the cytosol across the plasma membrane. Fe^{2+} is then converted to Fe^{3+} by a membrane-bound or soluble ferroxidase such as Cp or APP (shown). The absence of the ferroxidase results in decreased iron release into the extracellular space, as Fe^{2+} is unable to be converted into Fe^{3+}. APP ferroxidase is inhibited by extracellular Zn^{2+} (Figures 2A & 6B), which can exchange from Aβ:Zn^{2+} aggregates (Figure 6D). Free Zn^{2+} is normally buffered by the presence of ligands such as metallothioneins (including metallothionein III in the extracellular space), which are lost in AD (Uchida et al., 1991). Loss of metallothioneins and other Zn^{2+} buffers may lie upstream in amyloid pathology, APP ferroxidase inhibition and neuronal iron accumulation in AD. See also Figure S6.